Implication of mountain shading and topographic scaling on energy for snowmelt

Chris B. Marsh[1, 2], John Pomeroy[1], Raymond J. Spiteri[2]

1 Centre for Hydrology, Dept. Geography and Planning, University of Saskatchewan

2 Numerical Simulation Lab, Dept. Computer Science, University of Saskatchewan

Email: cbm038@mail.usask.ca

Abstract

In many parts of the world, snowmelt energetics are dominated by incoming solar radiation. This is the case in the Canadian Rockies, where sunny winters result in high insolation. Solar irradiance at the snow surface is affected by the atmosphere, the slope and aspect of the immediate topography, and shading from surrounding terrain. Errors in estimating solar irradiation are cumulative over a season and can lead to large errors in snowmelt predictions. Current gridded methods used to estimate solar irradiance in complex terrain work best with high-resolution DEMs, such as those produced using LiDAR. The requirement for high-resolution DEMs is a significant problem when modelling large spatial domains due to the lack of LiDAR elevation information over much of Canada. However, it is possible that adaptive triangular meshes, a type of unstructured triangular mesh that can adapt to fine-scale processes during model runtime, are more efficient in their use of DEM data than fixed grids when producing solar irradiance maps. A field and modelling study aimed at determining the effect of changes in DEM resolution on fixed grid and adaptive mesh irradiation calculations is discussed in this paper. As part of this study, the accuracy of these techniques is compared to measurements of mountain shadows and solar irradiance collected in the Marmot Creek Research Basin, Alberta. Time-lapse digital cameras and networks of radiometers provide datasets for diagnosis of model accuracy.

Introduction

In areas of variable topography, a surface's aspect significantly controls how much incident solar radiation a surface is exposed to. In a catchment in the Yukon, Canada, Pomeroy et al. (2003) found that on a clear day at midday, a south-facing surface had 80% more radiation than the north-facing surface. Carey and Woo (1998) found that aspect played a significant role in snowpack melt timing and attributed this as one factor that accentuates the contrast in timing and magnitude of the snowmelt between north and south facing slopes. Chueca and Julián (2004) found that shortwave radiation had implications for glacial ablation, concluding that the morphology and spatial distribution of small cirque glaciers could be primarily attributed to the differences in shortwave incoming radiation.

Structured meshes in GIS are generally referred to as rasters or grids. Raster based models are common because their computer representation can be trivially implemented using two dimensional arrays, a feature intrinsic to any modern programming language. Despite their widespread use, rasters have a number of significant limitations for use in hydrological modelling: drainage directions are often constrained to 45^o intervals, and geometric artifacts and other sub-grid variability can be artificially introduced because of the ridged structure (Tucker, 2001). Representing a non-rectangular

hydrological basin requires buffering around the basin in order to capture its irregular shape with regular cells. This can result in having to either mask areas out, compute values for areas not being used in the simulation, or focusing on a 'window' within the basin that can be fully captured via a raster, neglecting the rest of the basin. These problems can be partially mitigated when unstructured meshes are used for topographic representation.

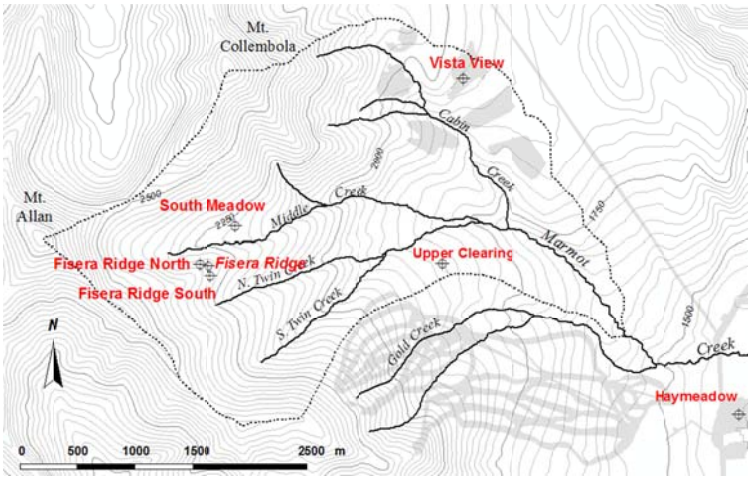

Figure 1: Marmot Creek Research basin, Alberta.

Research basin

The model domain for this project is Marmot Creek, shown in Figure 1, a research basin operated by the Centre for Hydrology, University of Saskatchewan in the Kananaskis Valley, Alberta. The basin ranges in elevation from approximately 1450 to 2886 m.a.s.l and is located at approximately 50^{o} 58'N and 115^{o} W. Vegetation is characterized by a combination of clear cut, meadow, forest, and alpine terrain. Shortwave pyranometers were placed at the indicated sites in Figure 1; Apogee SP-110s at Fisera Ridge North and South, South Meadow, Vista View, and Haymeadow; Kipp & Zonen CRN1s at Fisera Ridge and Haymeadow; and Delta-T SPN1s were installed at Fisera Ridge and Haymeadow. Two time-lapse cameras were installed; one at Fisera Ridge looking towards Mount Allan, and one at Fisera Ridge North facing Mount Collembola.

Figure 2: Time lapse photographs from Fisera Ridge north showing topographic shading. The red arrow shows the south meadow clearing site. Photos taken Nov 10, 2010 at 15:00 and 16:00.

Importance of shading

As noted above, slope and aspect is important for energy calculations. However, many studies do not considered shading of a surface from the surrounding terrain. As shown in Figure 2, sharp topographic shadows dramatically decrease the irradiance to a slope. The errors from failing to capture this process accumulate throughout the season.

Model development

A raster dataset, such as that derived from LiDAR, may be triangulated using Delaunay triangulation. Using this method, the triangulation could be constrained to the model domain, streams, or any other feature as required. Once the triangulation is constructed, shading locations can be mapped using, and expanding upon, the method proposed by Montero, et al. (2009). Other methods such as ray tracing are possible, however when working with arbitrarily orientated triangles it becomes difficult to know how many directions to look in. As the topographic scale changes, the look directions and collision tests must change, further increasing the uncertainty of the tests, and increasing the computational costs.

The method of Montero et al. (2009) determines shaded areas by determining what triangles are in front of other triangles with respect to the sun. To do this, the coordinate system is rotated so that the vertical coordinate (z) is rotated until it points at the sun. In this rotated configuration, some triangles may be located between the sun and other triangles, and therefore result in shading. Details of this rotation follow.

Let h_o be the solar elevation, and A_o be the solar azimuth (clockwise from north, in radians) for a certain time *t*. Then the vector defining the solar beam ($\vec{s}$) in terms of a unit spherical coordinate system is given by

$$\vec{s} = \begin{bmatrix} \cos h_o \sin A_o \\ \cos h_o \cos A_o \\ \sin h_o \end{bmatrix}.$$

Let *x,y,z* be a reference coordinate system with *x* positive in the east, *y* positive in the north, and *z* positive in the vertical direction that the topographic data is defined in. Let *x',y',z'* be a coordinate system obtained by performing an XZX Euler rotation of *x,y,z*.

Let R_x be the x rotation matrix and R_z be the z rotation matrix given as:

$$R_x = \begin{bmatrix} 1 & 0 & 0 \\ 0 & \cos\phi & -\sin\phi \\ 0 & \sin\phi & \cos\phi \end{bmatrix}$$

and

$$R_z = \begin{bmatrix} \cos\phi & -\sin\phi & 0 \\ \sin\phi & \cos\phi & 0 \\ 0 & 0 & 1 \end{bmatrix}.$$

Then the rotation from *x,y,z* to *x',y',z'* is done via the Euler rotation *E* where

$$E = R_x(-q_o)R_z(-z_0)R_x(0)$$

$$E = \begin{bmatrix} \cos z_o & \sin z_o & 0 \\ -\cos q_o \sin z_o & \cos q_o \cos z_0 & \sin q_o \\ \sin q_o \sin z_o & -\sin q_o \cos z_o & \cos q_o \end{bmatrix}.$$

Where, borrowing from Montero, et al. (2009), $q_o = \frac{\pi}{2} - h_o$ and $z_o = \pi - A_o$.

The rotation E is applied to each vertex of every triangle. Then the rotated triangles can be projected onto the x'y' plane by ignoring their z' values; that is, they are shown as 2D triangles. The triangles can then be coloured according to each of the 3 vertex's z' values. An example of this is shown in Figure 3; the colours represent the z' values of each triangle, ranging from blue for low, and red for high. The scene is shown with the observer between the sun and the terrain. No scale is given because the z' values are not physical values and are relative, denoting "closer to" the sun for high values, and "farther from" the sun for low values. This is shown from a different perspective in Figure 4, with the observer located looking approximately towards the sun.

Shadow detection

Montero et al. (2009) suggested constructing the entire triangulation via nested triangles. However, this does not

allow for constraining to hydrologically important features such as basin outlines, or streams. Therefore in this paper nested Rivara 4-T triangles (Rivara, 1987) will be used only after the Delaunay triangulation. In this approach, each Delaunay triangle is subdivided into 4 sub triangles following the algorithm proposed by Rivara (1987). Because of the nesting, it allows triangles to be refined and coarsened during model runtime without requiring a domain wide remeshing, nor changing the shape of the Delaunay triangles. Instead of starting with many small triangles, triangles can be refined as needed to capture shadow bounds, and coarsened when either fully in sun or shadow. This adaptive resolution is computationally more efficient and allows for capturing the shadow boundary accurately, even if the original dataset is not of a high resolution.

In order to determine which triangles are shaded, a centre for each sub-triangle is calculated and, if a sub-triangle centre lies within another non sub-triangle, a collision has occurred. This is done instead of triangle-triangle collision detection because it is computationally more efficient.

This recursive, sub-triangle representation allows for capturing the advancing front of the shadow. Montero et al. (2009) only considered one level of subdivision, as is currently done here. However future work will allow for multiple levels of adaptive division. This will allow each of the larger Delaunay triangles to contain an arbitrary number of smaller, nested triangles. An example binary shadow/no shadow map constructed using this method is shown in Figure 5. The locations A and B in Figures 3, 4 and 5 show areas that are expected to be shaded. As shown in Figure 3, B should be shaded and location B in Figure 5 confirms this. Although some numerical problems are visible in Figure 5 where triangles fail to be properly classified, this is attributed to the approximating triangle-triangle detection. This numerical precision will be fixed in future work.

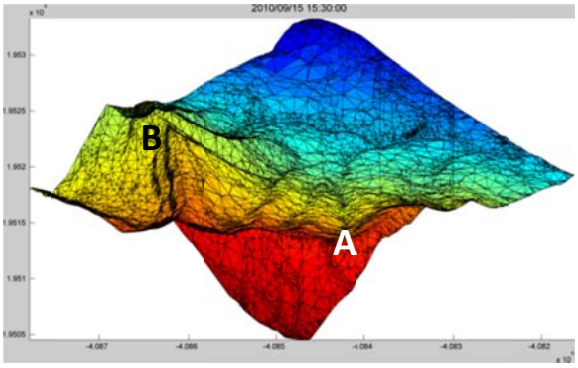

Figure 3: Domain projected onto x'y' coloured by z' values. Shown with the observer located between the sun and the terrain. The red values are "closer to" the sun and the blue values are "farther" from the sun. Model time: 15:30. Labels A and B discussed below.

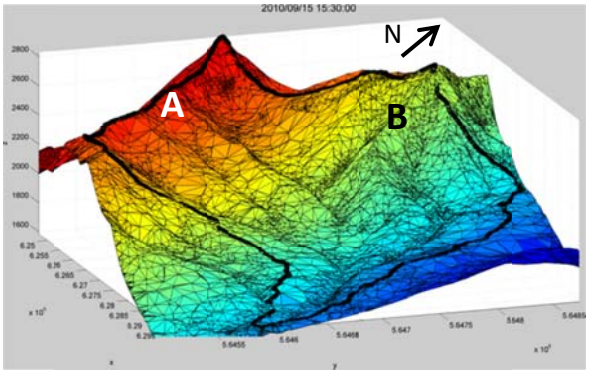

Figure 4: The red values are "closer to" the sun and the blue values are "farther" from the sun. This shows that the left most ridge-line has an opportunity to shade topography shown in shades of yellow or green for example. Model time: 15:30. Marmot Creek basin is outlined in black.

However, these are promising initial results as it shows a TIN without ray tracing creating topographic shadows from remote topographic features.

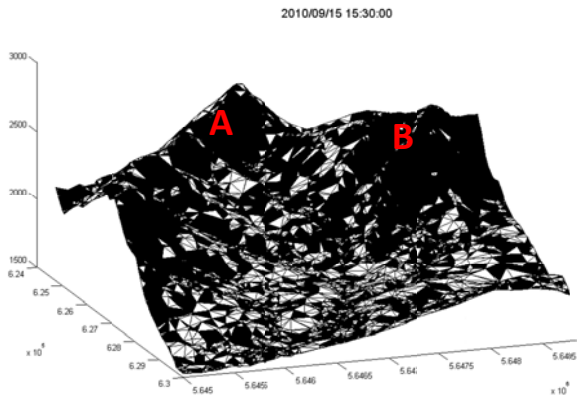

Figure 5: Binary shadow/no shadow map. The ridge line (A) in Figure 3 is clearly shown as shaded. Model time: 15:30

Verification

The model outputs, such as shown in Figure 5, will be compared to orthorectified imagery taken with the time lapse cameras. An example shot (not orthorectified) is shown in Figure 2. Once the imagery is orthorectified, image processing can determine the shadow bounds allowing for direct empirical comparison with model data. In addition, measured irradiance will be compared to model outputs of direct and diffuse beam for shadow and no-shadow areas. As well, a variety of existing shading codes will be run to determine the effects of spatial resolution on their predictions. Finally, as there has not been a systematic comparison of nested TIN codes described in the literature, the effect of resolution change on results will be investigated.

Conclusion

Raster representation of topography for hydrological purposes is not always ideal, and alternative data structures can mitigate most of the shortfalls. For example, utilizing adaptive meshes to capture sub-triangle shading can more efficiently utilize low resolution datasets. Utilizing ideas put forth by Montero, et al. (2009), an unstructured, adaptive mesh is used to capture shading without the need for ray tracing. These model data will be compared to orthorectified imagery to validate the model and help understand scaling effects. Further comparisons with measured irradiance will be done.

References

Carey S, Woo M-ko. Snowmelt hydrology of two subarctic slopes, southern Yukon, Canada. *Nordic Hydrology*. 1998;29(4):331

Chueca J., Julián A. Relationship between solar radiation and the development and morphology of small cirque glaciers (Maladeta Mountain massif, Central Pyrenees, Spain). *Geografiska Annaler: Series A, Physical Geography*. 2004;86(1):81-89.

Montero G, Escobar J, Rodriguez E, Montenegro R. Solar radiation and shadow modelling with adaptive triangular meshes. *Solar Energy*. 2009;83(7):998-1012.

Pomeroy JW, Toth B, Granger RJ, Hedstrom NR, Essery RLH. Variation in Surface Energetics during Snowmelt in a Subarctic Mountain Catchment. *Journal of Hydrometeorology*. 2003;4(4):702-719.

Rivara M-C. A grid generator based on 4-triangles conforming mesh-refinement algorithms. International Journal for Numerical Methods in Engineering. 1987;24(7):1343-1354.

Tucker G. An object-oriented framework for distributed hydrologic and geomorphic modeling using triangulated irregular networks. *Computers & Geosciences*. 2001;27(8):959-973.